Eur. Phys. J. B **38**, 83–91 (2004)
DOI: 10.1140/epjb/e2004-00102-5

THE EUROPEAN PHYSICAL JOURNAL B

Stiffness exponents for lattice spin glasses in dimensions d = 3, . . . , 6

S. Boettcher[a]

Physics Department, Emory University, Atlanta, Georgia 30322, USA

Received 29 October 2003
Published online 20 April 2004 –

Abstract. The stiffness exponents in the glass phase for lattice spin glasses in dimensions $d = 3, \ldots, 6$ are determined. To this end, we consider bond-diluted lattices near the $T = 0$ glass transition point p^*. This transition for discrete bond distributions occurs just above the bond percolation point p_c in each dimension. Numerics suggests that both points, p_c and p^*, seem to share the same $1/d$-expansion, at least for several leading orders, each starting with $1/(2d)$. Hence, these lattice graphs have average connectivities of $\alpha = 2dp \gtrsim 1$ near p^* and exact graph-reduction methods become very effective in eliminating recursively all spins of connectivity ≤ 3, allowing the treatment of lattices of lengths up to $L = 30$ and with up to $10^5 - 10^6$ spins. Using finite-size scaling, data for the defect energy width $\sigma(\Delta E)$ over a range of $p > p^*$ in each dimension can be combined to reach scaling regimes of about one decade in the scaling variable $L(p - p^*)^{\nu^*}$. Accordingly, unprecedented accuracy is obtained for the stiffness exponents compared to undiluted lattices ($p = 1$), where scaling is far more limited. Surprisingly, scaling corrections typically are more benign for diluted lattices. We find in $d = 3, \ldots, 6$ for the stiffness exponents $y_3 = 0.24(1)$, $y_4 = 0.61(2)$, $y_5 = 0.88(5)$, and $y_6 = 1.1(1)$.

PACS. 05.50.+q Lattice theory and statistics (Ising, Potts, etc.) – 64.60.Cn Order-disorder transformations; statistical mechanics of model systems – 75.10.Nr Spin-glass and other random models – 02.60.Pn Numerical optimization

1 Introduction

The stiffness exponent y (often labeled θ) is one of the most fundamental quantities to characterize the low-temperature state of a disordered spin system [1]. It provides an insight into the effect of low-energy excitations of such a system [2,3]. A recent study suggested the importance of this exponent for the scaling corrections of many observables in the low-temperature regime [4], and it is an essential ingredient to understand the true nature of the energy landscape of finite-dimensional glasses [5–7].

To illustrate the meaning of the stiffness exponent, one may consider an ordinary Ising ferromagnet of size L^d with bonds $J = +1$, which is well-ordered at $T = 0$ for $d > 1$, having periodic boundary conditions. If we make the boundary along one spatial direction anti-periodic, the system would form an interface of violated bonds between mis-aligned spins, which would raise the energy of the system by $\Delta E \sim L^{d-1}$. This "defect"-energy ΔE provides a measure for the energetic cost of growing a domain of overturned spins, which in a ferromagnet simply scales with the surface of the domain. In a disordered system, say, a spin glass with an equal mix of $J = \pm 1$ couplings, the interface of such a growing domain can take advantage of already-frustrated bonds to grow at a reduced or even vanishing cost. Defect energies will be distributed with zero mean, and the typical range, measured by the width of the distribution $\sigma(\Delta E)$, may scale like

$$\sigma(\Delta E) \sim L^y. \tag{1}$$

Clearly, it must be $y \leq d-1$, and a bound of $y \leq (d-1)/2$ has been proposed for spin glass systems generally [2]. Particularly, ground states of systems with $y \leq 0$ would be unstable with respect to spontaneous fluctuations, which could grow at no cost, like in the case of the one-dimensional ferromagnet where $y = d - 1 = 0$. Such a system does not manage to attain an ordered state for any finite temperature. Conversely, a positive sign for y at $T = 0$ indicates a finite-temperature transition into an ordered regime while its value is a measure of the stability of the ordered state. Furthermore, in a d-dimensional family of systems, the marginal value $y_{d_c} = 0$ provides the lower critical dimension d_c for such systems.

Accordingly, there have been many attempts to obtain the value of stiffness exponents in finite-dimensional spin glasses [7–17], using transfer matrix, optimization, or renormalization group techniques. In the early days of spin-glass theory, it was soon argued that $y < 0$ for $d \leq 2$ and $y > 0$ for $d \geq 3$ [8,11]. Only recently, though,

[a] e-mail: sboettc@emory.edu

the stiffness exponent for $d = 2$, below the lower critical dimension, has been improved to considerable accuracy, $y_2 = -0.282(2)$ [15,16]. There has still been little progress in the accurate determination of y_3 in the last 20 years, despite significant increases in computational power. It's value is expected to be small and positive, and so far has been assumed to be near $y_3 \approx 0.19$ [11,13], although there have been investigations recently pointing to a larger value, such as 0.23 [7] or 0.27 [15]. In some sense, all of these results are consistent, since they were obtained over exceedingly small scaling windows, $L = 6, \ldots, 12$ at best, and large errors have to be assumed. In $d = 4$ the only value reported to date has been $y_4 = 0.64(5)$ using $L \leq 7$ [14].

In this paper we use numerical investigations of $\pm J$ spin glasses on *dilute* lattices to obtain improved predictions for the stiffness exponents in dimensions $d = 3, \ldots, 6$. First, we explore such lattices near their bond-percolation transition p_c to find a separate transition $p^* > p_c$ into a $T = 0$ spin-glass state, as anticipated by references [17,18]. We find that p^* becomes ever closer to p_c for increasing d, both scaling with $1/(2d)$. Thus, near either transition, bond-diluted lattices have spins with connectivities distributed near $2dp^* \approx 1$. Such sparse graphs can be effectively reduced with a set of *exact* rules that eliminate a large fraction of spins, leaving behind a small, compact remainder graph that is easier to optimize. The increase in the scaling regime with lattice size, in combination with finite-size scaling techniques, leads to much improved or entirely new predictions for the stiffness exponents of low-dimensional lattices. In particular, we find that $y_3 = 0.24(1)$, $y_4 = 0.61(2)$, $y_5 = 0.88(5)$, and $y_6 = 1.1(1)$. Our value in $d = 3$ is at the higher end of most previous studies and amazingly close to (but distinct from) the value obtained with the Migdal-Kadanoff approximation, $y_3^{\mathrm{MK}} = 0.25546(3)$ [17]. The value for $d = 4$ is consistent with reference [14] and quite below the Migdal-Kadanoff value, $y_4^{\mathrm{MK}} = 0.76382(5)$. The value for the upper critical dimension, $d_u = 6$, may be consistent with unity. Yet, studies in even higher dimensions [19] indicates a further rise in y_d with d, which appears to agree with recent replica theory predictions for $d \geq 6$ [20], although the specific numerical values for y_d are significantly below those predictions.

In the following section, we discuss the observables that our numerical experiments measure, in Section 3 we describe the reduction rules for low-connected spins and the optimization method use in this study. Section 4 presents the results of the experiments for the threshold p^*, the correlation-length exponent, ν^*, for the transition into a glassy state for increasing bond density at p^*, and the stiffness exponent y, in each dimension. In Section 5 we conclude with a discussion regarding the d-dependence of y.

2 Determining stiffness exponents

To understand why the accurate determination of these stiffness exponents is such a challenging task, it is important to appreciate its complexity: Most numerical studies are based on sampling the variance

$$\sigma(\Delta E) = \sqrt{\langle \Delta E^2 \rangle - \langle \Delta E \rangle^2} \tag{2}$$

of the distribution of defect energies ΔE obtained via inverted boundary conditions (or variants thereof [15]), as described above. Thus, for an Ising spin glass with periodic boundaries, an instance of fixed, random bonds is generated, its ground-state energy is determined, then all bonds within a hyperplane have their sign reversed and the ground-state energy is determined again. The defect energy is the often-minute difference between those two ground state energies. Then, many such instances of a given size L have to be generated to sample the distribution of ΔE and its width $\sigma(\Delta E)$ accurately. Finally, $\sigma(\Delta E)$ has to be fitted to equation (1) for a sufficiently wide range of L in the asymptotic regime.

The most difficult part of this procedure, limiting the range of L that can be achieved, is the accurate determination of the ground state energies in the first place. While for $d \leq 2$ efficient algorithms exist to determine ground state energies exactly, and large system sizes can be obtained [15,16], for $d \geq 3$ no such algorithm exists: Finding ground states is known to be an NP-hard optimization problem [21] with the cost of any exact algorithm likely to rise faster than any power of L. There have been a variety of accurate measurements of ground-state energies [22–24] using heuristic methods. In these measurements small systematic errors in failing to obtain a ground state tend to submerge beneath the statistical error. In contrast, for the defect energy the extensive leading-order contributions to the ground states are subtracted out, and such systematic failings may surface to dominate any statistical errors. Accordingly, system sizes that can be approximated with heuristics may turn out to be far more limited than one may have anticipated based on those previous studies.

To increase the range of system sizes L without increasing the optimization problem, we observe that a bond-diluted lattice will have the same defect energy scaling as a fully connected lattice. Above the finite-size scaling window for bond-percolation near p_c, the dominant cluster embedded on the lattice is a compact structure with the same long-range properties of the fully connected lattice. Similarly, the spin-glass problem defined on that cluster should exhibit the same long-range behavior as the undiluted lattice glass at $T = 0$, their difference being of a short-range geometric nature. Hence, for all bond densities p above the scaling window of the $T = 0$ glass transition, equation (1) should be applicable. Yet, a spin glass on a bond-diluted lattice in turn can be expected to be less frustrated, up to the point that frustration fails to create long-range correlated behavior. This is certainly the case below the bond-percolation transition p_c, where any defects should remain localized. Thus we focus on the regime somewhere above p_c, where the system can exhibit spin-glass behavior but where we may take advantage of the weakened frustration to optimize larger system sizes L.

As another feature of our new approach, the introduction of a new control parameter, the bond density p,

permits a finite size scaling Ansatz. Combining the data for all L *and* p leads to a new variable which has the chance of exhibiting scaling over a wider regime than L alone. As has been argued in reference [18], we can make an Ansatz of

$$\sigma(\Delta E) \sim \mathcal{Y}\, L^y g\left[L\,(p-p^*)^{\nu^*}\right], \tag{3}$$

where $\mathcal{Y} \sim \mathcal{Y}_0(p-p^*)^f$ refers to the surface tension, which must vanish for $p \to p^*$, and g is a scaling function in the new scaling variable, $x = L\,(p-p^*)^{\nu^*}$. The exponent ν^* describes the divergence of the correlation length for the transition into the ordered state at p^*. (In the Migdal-Kadanoff approximation, it was found that ν^* is larger than ν of the percolation transition [18].) Scale invariance at $p \to p^*$ dictates $f = y\nu^*$, and in terms of the scaling variable x we have

$$\sigma(\Delta E) \sim \mathcal{Y}_0\, x^y g(x). \tag{4}$$

We will use the finite-size scaling relation in equation (4) to analyze our data in Section 4.2. In the following section, we describe the new algorithm for spin glasses on dilute lattices, which at $T = 0$ traces out many weakly connected spins to leave a much reduced remainder graph that can be optimized subsequently by other means.

3 Reduction algorithm for the energies

We will describe the reduction algorithm for spin glasses on general sparse graphs at $T = 0$ in more detail elsewhere [25], including its ability to compute the entropy density and overlap (see also [17]). We focus here exclusively on the reduction rules for the ground state energy. We have used these reduction rules previously for large three-connected Bethe lattices [26]. These rules apply to general Ising spin glass Hamiltonians

$$H = -\sum_{\langle i,j\rangle} J_{i,j}\, x_i\, x_j, \quad (x_i = \pm 1), \tag{5}$$

with any bond distribution $P(J)$, discrete or continuous, on arbitrary sparse graphs. Here, we use exclusively a $\pm J$ bond distribution, and bond-diluted hyper-cubic lattices in $d \geq 3$. A Gaussian or any other distribution with zero mean and unit variance is expected to yield the same value of y [4]. Our preliminary experiments with a Gaussian distribution have shown faster converging averages at a given L, but more persistent scaling corrections for increasing L.

The reductions effect both spins and bonds, eliminating recursively all zero-, one-, two-, and three-connected spins and their bonds, but also adding new bonds between spins which may or may not have been connected previously. These operations eliminate and add terms to the expression for the Hamiltonian in equation (5), leaving it *form-invariant*. Offsets in the energy along the way are accounted for by a variable H_o, which is *exact* for at $T = 0$.

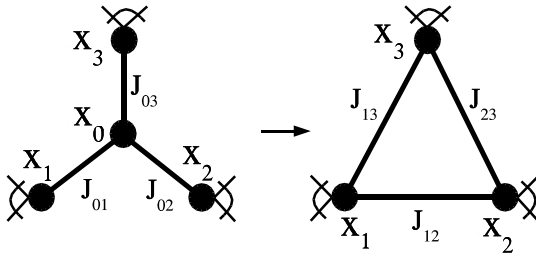

Fig. 1. Depiction of the "star-triangle" relation to reduce a three-connected spin (x_0, center-left). The values for the new bonds on the right are obtained in equation (9).

Rule I: An isolated spin, which does not contribute to the sum in equation (5) at all, can be eliminated without changing that sum.

Rule II: A one-connected spin i can be eliminated, since its state can always be chosen in accordance with its neighboring spin j to satisfy the bond $J_{i,j}$, i.e. in the only term in equation (5) relating to x_i,

$$x_i\, x_j\, J_{i,j} \leq |J_{i,j}| \tag{6}$$

we can always choose x_i to saturate the bound, which is the energetically most favorable state. With that, we adjust $H_o := H_o - |J_{i,j}|$ and eliminate the term $-J_{i,j}\, x_i\, x_j$ from H.

Rule III: A double bond, $J_{i,j}^{(1)}$ and $J_{i,j}^{(2)}$, between two vertices i and j can be combined to a single bond by setting $J_{i,j} = J_{i,j}^{(1)} + J_{i,j}^{(2)}$ or be eliminated entirely, if the resulting bond vanishes. This operation is very useful, since it lowers the connectivity of i and j at least by one. Particular to discrete bond distributions, there is a finite probability that the two original bonds cancel each other ($J_{i,j} = 0$), which may entirely *disconnect* i and j and reducing their connectivity by two. (Double bonds are absent from the original lattice but may arise via the recursive application of these reduction rules.)

Rule IV: For a two-connected spin i, its two terms in equation (5) can be rewritten

$$\begin{aligned} J_{i,1}x_ix_1 + J_{i,2}x_ix_2 &= x_i(J_{i,1}x_1 + J_{i,2}x_2) \\ &\leq |J_{i,1}x_1 + J_{i,2}x_2| \\ &= J_{1,2}x_1x_2 + \Delta H, \end{aligned} \tag{7}$$

with

$$\begin{aligned} J_{1,2} &= \frac{1}{2}\left(|J_{i,1} + J_{i,2}| - |J_{i,1} - J_{i,2}|\right), \\ \Delta H &= \frac{1}{2}\left(|J_{i,1} + J_{i,2}| + |J_{i,1} - J_{i,2}|\right), \end{aligned}$$

leaving the graph with a new bond $J_{1,2}$ between spin 1 and 2, and acquiring an offset $H_o := H_o - \Delta H$.

Rule V: A three-connected spin i can be reduced via a "star-triangle" relation (see Fig. 1):

$$\begin{aligned} & J_{i,1}x_ix_1 + J_{i,2}x_ix_2 + J_{i,3}x_ix_3) \\ &= x_i\,(J_{i,1}x_1 + J_{i,2}x_2 + J_{i,3}x_3) \\ &\leq |J_{i,1}x_1 + J_{i,2}x_2 + J_{i,3}x_3| \\ &= J_{1,2}x_1x_2 + J_{1,3}x_1x_3 + J_{2,3}x_2x_3 + \Delta H, \end{aligned} \tag{8}$$

with

$$J_{1,2} = -A - B + C + D, \quad J_{1,3} = A - B + C - D,$$
$$J_{2,3} = -A + B + C - D, \quad \Delta H = A + B + C + D,$$
$$A = \tfrac{1}{4}\left|J_{i,1} - J_{i,2} + J_{i,3}\right|, \quad B = \tfrac{1}{4}\left|J_{i,1} - J_{i,2} - J_{i,3}\right|,$$
$$C = \tfrac{1}{4}\left|J_{i,1} + J_{i,2} + J_{i,3}\right|, \quad D = \tfrac{1}{4}\left|J_{i,1} + J_{i,2} - J_{i,3}\right|.$$

The bounds in equations (6–9) are saturated for the right choice of the spin x_i that links the terms together, thus optimizing its alignment with the local field as is required when the remaining graph takes on its ground state. In turn, for $T > 0$ the eliminated spin x_i may not take on its own energetically most favorable state to minimize the *free* energy of the configuration instead. Hence, the reduction algorithm is exact only in determining the ground state.

Reducing four- and higher-connected spins would lead to new bonds that connect more than 2 spins, creating in general a hyper-graph with multi-spin interaction terms. For instance, a term in H connecting a spin x_0 to four other spins would be replace by one term connecting all four, six terms mutually connecting the four neighbors in all possible pairs, and an energy offset[1]. While such a strategy may be useful, we will confine ourselves here to reductions producing only new two-spin interactions.

It is important that these rules are applied recursively and in the given order. That is, one may only apply *Rule II* after there are no more spins reducible by *Rule I*, apply *Rule III* only after both, *Rule I* and *Rule II*, have been exhausted, etc. And after the application of any higher rule, it needs to be checked if structures have been generated to which any lower rule may now apply. For example, the recursion may have generated a spin that is two-connected, but via a double bond to a single other spin. Applying *Rule IV* to that spin before *Rule III* would lead to the other spin having a bond onto itself, a problematic situation for which we have no rule. In any event, even if we had provided more rules for all eventualities, it is still far more efficient to first reduce the lowest connected spin at any one time.

After all these rules have been exhausted, the original lattice graph is either completely reduced (which is almost certainly the case for $p < p_c$), in which case H_o provides the exact ground state energy already, or we are left with a much reduced, compact graph in which no spin has less than four connections. Note that bonds in the remainder graph may have properties uncharacteristic of the original bond distribution. For example, $\pm J$-bonds may have combined to bonds of any integer multiple of J (e.g. via *Rule III*). Here, we obtain the ground state energy of the reduced graph with the extremal optimization heuristic [24], which together with H_o provides a very accurate approximation to the ground state energy of the original diluted lattice instance. Clearly, we could have just as well used other heuristics or exact methods to treat the remainder graph.

[1] As long as H only contains terms connecting an even number of spins, the reduction will preserve that evenness.

4 Numerical results

The following data was obtained during a window of about two months on a cluster of 15 Pentium4 PC running at 2.4 GHz with 256 MB of RAM.

The runtime of the EO heuristic was fixed to grow as $(n/5)^3$ with the number n of spin variables in the remainder graph after the reduction had been applied. In reference [24] it was found that typically $O(n^4)$ updates for instances up to $n \sim 10^3$ were needed to obtain consistently reproducible ground state energies. Since we are aiming at much larger statistics and typically smaller instances in the present study, we opted for a more limited runtime. Instead, an adaptive multiple restart system was used such that for each instance at least 3 runs from fresh random initial spin configurations were undertaken. If a new best-so-far configuration is found in run r, at least a total of $2r$ restarts would be applied to these more demanding instances [27]. For instances with $n > 700$ apparent inaccuracies in sampling the *difference* between ground state energies, ΔE, become noticeable.

For highly connected graphs with few spins to reduce, local search with the EO heuristic dominated by far the computational time. Our implementation of the reduction algorithm, originally conceived with $d = 3$ lattices with up to $L = 30$ in mind, started contributing significantly to the computational cost for instances with $L^d > 10^5$, hence most noticeably in the study of p^* in $d = 5$ and 6.

4.1 Determination of p*

In reference [18] it was shown that spin glasses on diluted lattices may possess a distinct critical point p^* in their bond fraction, which arises from the (purely topological) percolation threshold p_c of the lattice in conjunction with a discrete distribution of the bond weights $P(J)$. Clearly, no long-range correlated state can arise below p_c. A critical point distinct from percolation, $p^* > p_c$, emerges when such an ordered state above p_c remains suppressed due to collaborative effects between bonds [18] (see *Rule III* in Sect. 3). Just above p_c, the infinite bond-cluster is very filamentary and may easily be decomposed into finite components through such collaborative effects, involving a small number of bonds along narrow "bridges" between those components. Thus, to observe the onset of glassy properties on a dilute lattice, we have to cross another threshold $p^* \geq p_c$ first. In reference [17], we were able to locate p^* for the Migdal-Kadanoff lattice in accordance with theory [18] by using the defect energy scaling from equation (1): For all $p > p^*$ the stiffness exponent y eventually took on its $p = 1$ value, while for any $p < p^*$ defect energies diminished rapidly for increasing L.

In each dimension, we have run the above algorithm on a large number of graphs (about $10^5 - 10^6$ for each L and p) for p increasing from p_c in small steps. For each given p, L increased until it seemed clear that $\sigma(\Delta E)$ would either drop or rise for good. In this way, we bracket in p^*, as shown in Figure 2. Both, the bond-percolation

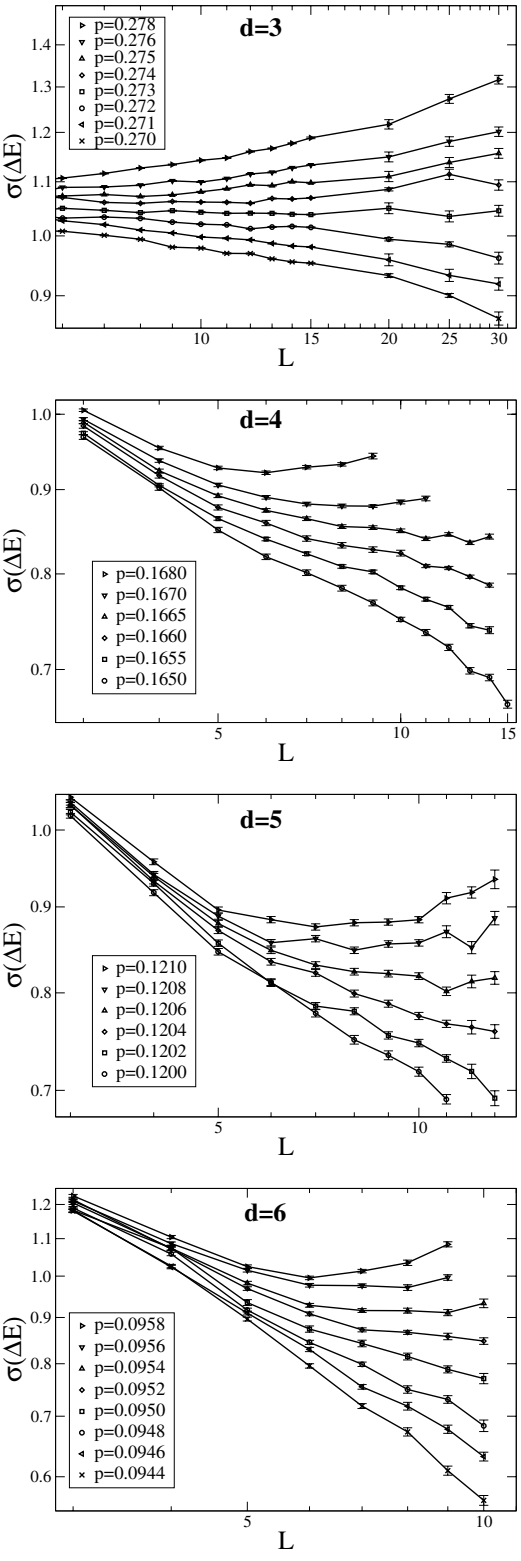

Fig. 2. Plot on a logarithmic scale of the variance $\sigma(\Delta E)$ of the defect energy as a function of systems size L for various bond fractions $p > p_c$ in $d = 3$ to 6. In each case, $\sigma(\Delta E)$ drops to zero rapidly for increasing L at smaller p, but turns around and rises for larger p, indicative of a nontrivial glassy state at low T. Near p^*, $\sigma(\Delta E)$ undergoes ever longer transients. The values for the thresholds p^* as suggested by the plots are listed in Table 1.

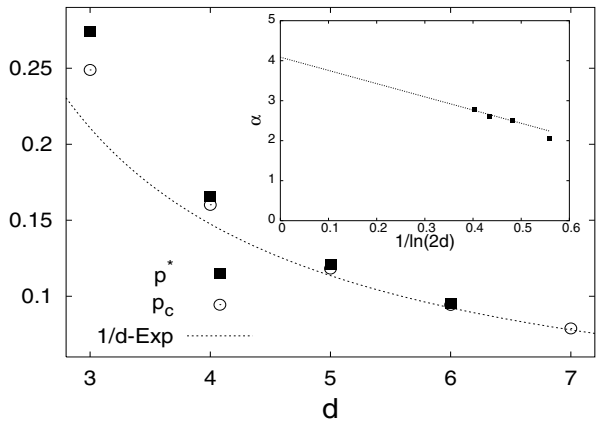

Fig. 3. Plot of the known bond-percolation thresholds p_c, the $T = 0$ glass transition thresholds p^* determined in Figure 2, and the $1/d$-expansion of p_c in equation (9) as a function of d. The insert shows $\ln(p^* - p_c)/\ln(2d)$ vs. $1/\ln(2d)$, extrapolating seemingly toward $\alpha \geq 4$ as in equation (10).

Table 1. List of the bond-density thresholds on hyper-cubic lattices for percolation p_c (taken from Ref. [28]) and for the $T = 0$-transition into a spin glass state, p^*, as determined from Figure 2. The values of p^* are dependent on the bond distribution which is $\pm J$ here.

d	p_c	p^*
3	0.2488	0.272(1)
4	0.160130	0.1655(5)
5	0.118174	0.1204(2)
6	0.0942	0.0952(2)

thresholds p_c, taken from reference [28], and our results for p^* are listed in Table 1.

It is interesting to compare the values of p^* to those of p_c for increasing dimension d. In Figure 3 we plot both, p_c and p^*, as a function of d, together with the prediction of the three-term $1/d$ expansion [29]

$$p_c \sim \frac{1}{2d} + \left(\frac{1}{2d}\right)^2 + \frac{1}{2}\left(\frac{1}{2d}\right)^3. \qquad (9)$$

The difference $p^* - p_c$ clearly decreases for $d \to \infty$. Assuming

$$p^* - p_c \sim (2d)^{-\alpha} \quad (d \to \infty), \qquad (10)$$

we plotted $\ln(p^* - p_c)/\ln(2d)$ vs. $1/\ln(2d)$ in the insert of Figure 3 to extrapolate for α. This crude extrapolation suggests $\alpha \geq 4$, so that p^* may share the $1/d$-expansion of p_c in equation (9), at least up to the given order. In any case, a bond-diluted lattice system with discrete $\pm J$ bonds enters its spin glass phase at an average connectivity $2dp^* \approx 1$, and the reduction methods outlined in Section 3 should be very effective in *any* sufficiently large dimension for $p \gtrsim p^*$.

The value of p^* is distribution-dependent [18], and the values determined here and listed in Table 1 result from discrete $\pm J$-bonds. It is expected that $p^* = p_c$ for any continuous distribution. The precise values for p^*, while

interesting in their own right, are not important for the following discussion of the defect energy scaling. We merely need to ensure a selection of bond densities sufficiently *above* p^*, where we would expect equation (1) to hold, and sufficiently close to p^* for an effective application of the reduction rules in Section 3.

4.2 Determination of defect energy scaling

We have conducted extensive numerical experiments to extract the asymptotic scaling of $\sigma(\Delta E)$ for a many conveniently chosen bond densities p, especially in $d = 3$, but also in higher dimensions, up to the upper critical dimension $d = 6$ [1]. As mentioned in Section 2, an appropriate choice of p is crucial to ensure a good compromise between maximal algorithmic performance (for smaller $p > p^*$) and minimal scaling corrections (for larger p) that maximizes the actual scaling window. While we can estimate the effect of p on the performance of our algorithm, we have a-priori no information about scaling corrections. We will see that scaling corrections are indeed large for $p \to p^*$. Yet, as luck will have it, they diminish rapidly for intermediate values of p and again *increase* for $p \to 1$ (at least in lower dimensions, where this limit was considered).

For the study of p^*, in principle very large system sizes can be reached due to the complete reduction of very sparse graphs. Since optimizing the spin glass on the remainder graph is an NP-hard problem, we have obtained more limited maximal system sizes above p^*, dependent of the bond density p. We obtained sizes ranging up to $L = 30$ at $p = 0.28$ to $L = 9$ at $p = 1$ in $d = 3$, $L = 15$ at $p = 0.18$ to $L = 5$ at $p = 1$ for $d = 4$, $L = 13$ at $p = 0.125$ to $L = 5$ at $p = 0.22$ in $d = 5$, and $L = 9$ at $p = 0.1$ to $L = 4$ at $p = 0.17$ in $d = 6$. For each choice of L and p, we have sampled the defect energy distribution with typically $N \approx 10^4 - 10^5$ instances, then determined its variance $\sigma(\Delta E)$. For each data point for $\sigma(\Delta E)$ the error bar is $\approx 5 - 10/\sqrt{N}$. In Figure 4, we plot all the data for each dimension simply according to equation (1), on a logarithmic scale. For most sets of graphs, a scaling regime (linear on this scale) is visible. Yet, various deviations from scaling can be observed. Clearly, each sequence of points should exhibit some form of small-size corrections to scaling for smaller L. For large L, the inability to determine defect energies correctly (according to the discussion in Sect. 2), will inevitably lead to a systematic bias in σ. Some data sets did not exhibit any discernible scaling regime whatsoever, most notably our data set for the undiluted lattice in $d = 3$.

To obtain an optimal scaling collapse of the data, we focus on the data inside the scaling regime for each set. To this end, we chose for each data set a lower cut in L by inspection. An appropriate high-end cut is introduced by eliminating all data points for which the remainder graph had a typical size of > 700 spins; at that point the EO heuristic (within the supplied runtime) seems to fail in determining defect energies with sufficient accuracy. All the remaining data points for L and p are fitted to a

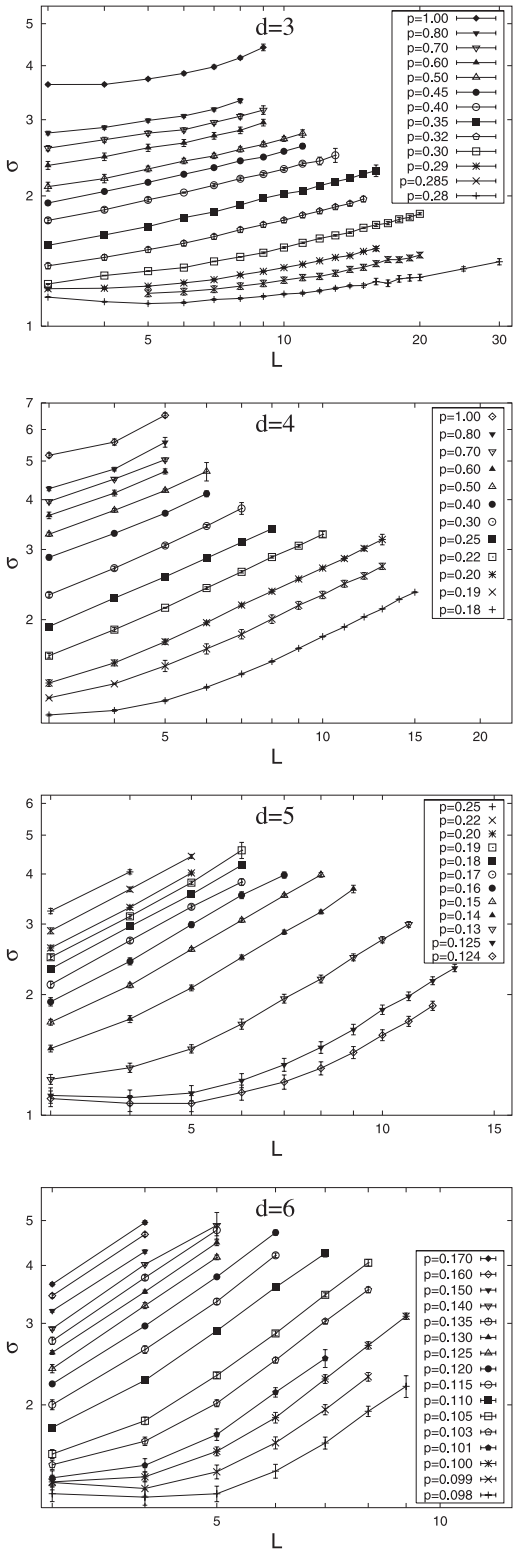

Fig. 4. Plot on a logarithmic scale of the width σ of the defect energy distribution as a function of system size L. From top to bottom, the data for dimensions $d = 3$, $d = 4$, $d = 5$, and $d = 6$ is shown. The data is grouped into sets (connected by lines) parameterized by the bond density p. Most sets show a distinct scaling regime as indicated by equation (1) for a rang of L above finite scaling corrections but below failing accuracy in the optimization heuristic.

Table 2. List of the fitted values for the critical bond-density p^*, the correlation-length exponent ν^*, the surface tension Υ_0, and the stiffness exponent y in each dimension $3 \leq d \leq 6$. Included is also the Q-value for each fit. The values for p^* here are bound to be less accurate than those directly determined in Section 4.1, but are consistent. In contrast, the values for y are quite stable.

d	p^*	ν^*	Υ_0	y	Q (DoF)
3	0.2706	1.17	2.37	0.239	1.00 (92)
4	0.1699	0.60	2.43	0.610	0.00 (47)
5	0.1217	0.50	3.05	0.876	0.86 (48)
6	0.0959	0.44	3.87	1.103	0.02 (46)

four-parameter scaling form,

$$\sigma(\Delta E) \sim \Upsilon_0 \left[L \left(p - p^* \right)^{\nu^*} \right]^y , \qquad (11)$$

i.e. approximating the scaling function $g(x)$ from equation (4) merely by unity, its leading behavior for large argument. Unfortunately, we have no knowledge of the functional form for finite-size corrections, making the low-L cut on the data a necessity. In Table 3 we have listed the number of instances N averaged over *only* for those (p, L)-data points that were judged to be in the scaling window. Note that *all* data above the low-L and below the high-L cut for each p was kept unaltered.

The fitted values for this and the other fitting constants (p^*, ν^*, and y) are listed in Table 2. Holding p^* fixed at the independently determined values from Table 1 reduces the variance in the remaining fitting parameters without changing much in their quoted values. Using the parameters of this fit, we re-plot only the data from the scaling regime in each dimension in Figure 5.

In each case, a convincing scaling collapse is obtained. Clearly, our data for $d = 3$ is not only the most extensive, but also happens to scale over nearly two decades without any discernible deviation or trend away from pure power-law scaling that would betray any systematic bias or lack of asymptotic behavior. This justifies a certain degree of confidence to project $y_3 = 0.24(1)$ for the scaling exponent where the quoted error is based on the uncertainty in the fit. Troublesome is the observation that the data for the undiluted lattice ($p = 1$) never reaches the scaling regime (see Fig. 5, top). This may be in accordance with the observation of reference [30], which found very long transients in a similar study on undiluted Migdal-Kadanoff lattices (see also Ref. [17]), or similar findings for undiluted lattices [31]. In our data, systematic errors in sampling ground states seem to set in for large L, before any scaling regime is reached at all.

For increasing dimension d, accessible scaling regimes become shorter, leading to more difficulty in determining an accurate fit of the power law. In $d = 4$ we can still claim scaling for about a decade in the scaling variable, justifying a prediction of $y_4 = 0.61(2)$. In $d = 5$ and $d = 6$, we only reach scaling windows significantly shorter than a decade. Luckily, y_d increases with increasing d, thus larger absolute errors still result in acceptable relative errors, and we predict from the fits in Figure 5 that $y_5 = 0.88(5)$ and $y_6 = 1.1(1)$.

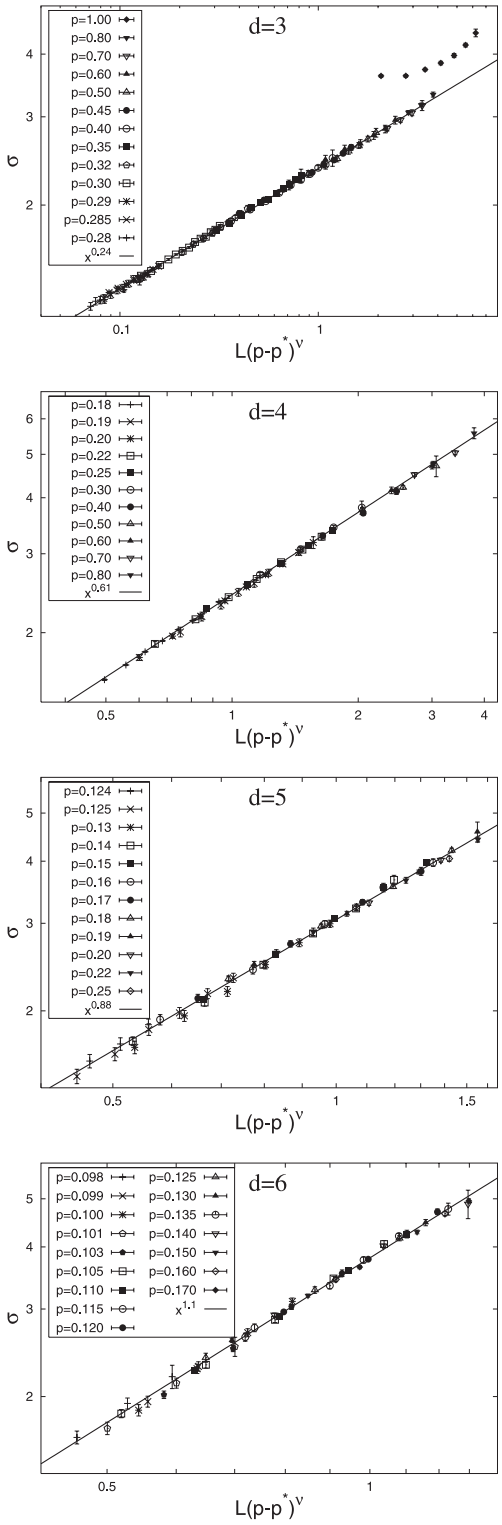

Fig. 5. Scaling plot of the data from Figure 4 for σ, fitted to equation (11) as a function of the scaling variable $x = L(p - p^*)^{\nu^*}$. Data above or below the scaling regime in each set from Figure 4 was cut. From top to bottom, the scaling collapse of the data for dimensions $d = 3$ to 6 is shown. The lines represent a power-law fit of the collapsed data which provides an accurate determination of the stiffness exponent y in each dimension. For $d = 3$ (top), we have also included the data for $p = 1$, which does not appear to connect to the scaling regime.

Table 3. Listing of the number of instances optimized at the bond densities p and system sizes L in Figure 4 that are actually used in Figure 5. Data points displayed in Figure 4 but left blank in this list were judged to be outside of the scaling regime either because of too small L to be asymptotic or because the remainder graph was too large ($n > 700$) to be accurately optimized.

		L																		
d	p	3	4	5	6	7	8	9	10	11	12	13	14	15	16	17	18	19	20	25	30
3	0.28															1e5	1e5	1e5	1e5	2e5	9e4
	0.285										1e5	1e5	1e5	1e5	1e5	1e5	1e5	1e5	1e5		
	0.29							2e6	2e6	2e6	2e6	2e6	1e6	1e6	1.8e5						
	0.3						1e7	1.2e6	1.2e6	1.2e6	1.2e6	1.2e6	1.2e6	1.2e6	2.5e5	2.5e5	2.5e5	2.5e5	2.5e5		
	0.32					1e5	1e5	1e5	1e5	1e5	1e5	1e5	1e5	1e5							
	0.35				1.25e6	1.25e6	1.25e6	2.4e5	2.4e5	2.4e5	1.6e5	1e5	1e5	1e5	1e4						
	0.4		1e5	1e5	1.2e6	1.2e5	1.2e5	1.2e5	1.2e5	1e5	2e5	6e3									
	0.45	1.2e5	1.2e5	1.2e5	1.2e5	1.2e5	1.2e5	1.2e5	1e5	5e4											
	0.5		4e4	4e4	4e4	4e4	4e4	4e4	4e4	1.6e4											
	0.6		2e4	2e4	2e4	2e4	2e4	2e4													
	0.7				5e4	5e4	5e4	1e4													
	0.8				7e4	7e4	3.5e4														
4	0.18							2.4e6	2.4e6	2.4e6	2.4e6	2.4e6	2.4e6	1.2e6							
	0.19						2e4	2e4	2e4	2e4	2e4	2e4									
	0.20			1.1e5	1.1e5	1.1e5	1.1e5	1.1e5	1.1e5	6e4	3e4	5e3									
	0.22		1.5e5	1.5e5	1.5e5	1.5e5	1.5e5	8.5e4	1.6e4												
	0.25		1.3e6	6.2e5	6.2e5	2e5	4e4														
	0.3		5e4	5e4	5e4	3e3															
	0.4		3e4	2.5e4	1e4																
	0.5		3e4	3e4	1e4																
	0.6		1e4	1e4																	
	0.7		3e4	1.7e4																	
	0.8		3e4	2e3																	
5	0.124							2e4	2e4	2e4	2e4										
	0.125						2e4	2e4	2e4	2e4	2e4	2e4									
	0.13				2e4	2e4	2e4	2e4	2e4	2e4											
	0.14		4e4	4e4	4e4	4e4	4e4	8e3													
	0.15		4e4	4e4	4e4	4e4	2e4														
	0.16	2e4	2e4	2e4	1e4	1e4															
	0.17	3e4	3e4	3e4	1e4																
	0.18	5e4	5e4	5e4	1e4																
	0.19	4e4	4e4	4e4	1e3																
	0.2	3e4	3e4	3e4																	
	0.22	2e4	2e4	2e4																	
	0.25	2e4	2e4																		
6	0.098					2e4	2e4	3.5e3													
	0.099					2e4	2e4														
	0.1				2e4	2e4	2e4	2e4													
	0.101			2e4	2e4	4e3															
	0.103			4e4	4e4	4e4															
	0.105		4e4	4e4	4e4	4e4	1e4														
	0.11		1.3e5	8e4	5e4	1e4															
	0.115		2e4	2e4	2e4																
	0.12		1.1e5	1e5	1.3e4																
	0.125	2e4	2e4	2e4																	
	0.13	8e4	6e4	1.2e4																	
	0.135	2e4	2e4	3e3																	
	0.14	1.1e5	5e4																		
	0.15	1e5	3.5e4																		
	0.16	4e4	2e4																		
	0.17	6e4	2.2e4																		

5 Conclusions

We have used the combined effort of an exact reduction method and an efficient heuristic to determine the defect energy distribution for $\pm J$-spin glasses on bond-diluted lattices in low dimensions. A subsequent finite size scaling fit of the data allowed us to extract the stiffness exponents in these dimensions to within 4% to 10% accuracy. Our approach also allowed the determination of a variety of other observables associated with the $T = 0$ transition into a glassy state at a bond-density p^* for $d \geq 3$. We hope that the methods introduced here may be applicable as well to the treatment of other open questions regarding the low-temperature state of spin glass systems [5,6].

Our value of $y_3 = 0.24(1)$ in $d = 3$ is near the higher end of previous estimates varying between 0.19 and 0.27, while $y_4 = 0.61(2)$ in $d = 4$ overlaps with a previous result of 0.64(5) from reference [14]. There has been no previous value to compare with for $d = 5$ or $d = 6$, the upper critical dimension, but replica theory [20] would indicate a faster increase in the value of y_d with d than was found here.

There has been no previous determination of the exponents ν^*, except that it is bound to exceed the value of ν for percolation [18], and that its mean field value for $d \geq 6$ should be $\nu^*_\infty = 1/2$. In light of the fact that $\nu = 0.875$, 0.68, 0.57, and 0.5 for bond percolation in $d = 3$ to 6 [32], most of our fitted values for ν^* do not seem to satisfy these expectations, which is easily explained by their poor accuracy. For instance, $\nu^* \geq 1/2$ should hold, so it appears that the fitted values of ν^* are generally too low.

I would like to thank A. Percus, R. Palmer, M. Palassini, and A. Hartmann for helpful discussions, and our IT staff for providing access to our student computing lab. This project is supported by grant 0312510 from the Division of Materials Research at the National Science Foundation.

References

1. K.H. Fischer, J.A. Hertz, *Spin Glasses* (Cambridge University Press, Cambridge, 1991)
2. D.S. Fisher, D.A. Huse, Phys. Rev. Lett. **56**, 1601 (1986)
3. A.J. Bray, M.A. Moore, Phys. Rev. Lett. **58**, 57 (1987)
4. J.-P. Bouchaud, F. Krzakala, O.C. Martin, Phys. Rev. B **68**, 224404 (2003)
5. F. Krzakala, O.C. Martin, Phys. Rev. Lett. **85**, 3013 (2000)
6. M. Palassini, A.P. Young, Phys. Rev. Lett. **85**, 3017 (2000)
7. M. Palassini, A.P. Young, Phys. Rev. Lett. **83**, 5126 (1999)
8. B.W. Southern, A.P. Young, J. Phys. C **10**, 2179 (1977)
9. S. Kirkpatrick, Phys. Rev. B **15**, 1533 (1977)
10. J.R. Banavar, M. Cieplak, Phys. Rev. Lett. **48**, 832 (1982)
11. A.J. Bray, M.A. Moore, J. Phys. C **17**, L463 (1984)
12. M. Cieplak, J.R. Banavar, J. Phys. A **23**, 4385 (1990)
13. A.K. Hartmann, Phys. Rev. E **59**, 84 (1999)
14. A.K. Hartmann, Phys. Rev. E **60**, 5135 (1999)
15. A.C. Carter, A.J. Bray, M.A. Moore, Phys. Rev. Lett. **88**, 077201 (2002)
16. A.K. Hartmann, A.J. Bray, A.C. Carter, M.A. Moore, A.P. Young, Phys. Rev. B **66**, 224401 (2002)
17. S. Boettcher, Eur. Phys. J. B **33**, 439 (2003)
18. A.J. Bray, S. Feng, Phys. Rev. B **36**, 8456 (1987)
19. S. Boettcher, *Low-Temperature Excitations of Dilute Lattice Spin Glasses,* `cond-mat/0303431`
20. T. Aspelmeier, M.A. Moore, A.P. Young, Phys. Rev. Lett. **90**, 127202 (2003)
21. F. Barahona, J. Phys. A **15**, 3241 (1982)
22. K.F. Pal, Physica A **223**, 283 (1996); K.F. Pal, Physica A **233**, 60 (1996)
23. A.K. Hartmann, Phys. Rev. B **59**, 3617 (1999)
24. S. Boettcher, A.G. Percus, Phys. Rev. Lett. **86**, 5211 (2001)
25. S. Boettcher, A.G. Percus, in preparation
26. S. Boettcher, Phys. Rev. B **67**, R060403 (2003)
27. S. Boettcher, A.G. Percus, *Extremal Optimization at the Phase Transition of the 3-Coloring Problem*, Phys. Rev. E (to appear), `cond-mat/0402282`
28. B.D. Hughes, *Random Walks and Random Environments,* Vol. 2 (Clarendon, Oxford, 1996)
29. T. Hara, G. Slade, Comb., Prob. & Comp. **4** 197 (1995)
30. B. Drossel, M.A. Moore, Eur. Phys. J. B **21**, 589 (2001)
31. A.A. Middleton, Phys. Rev. B **63**, 060202(R) (2001); A.K. Hartmann, M.A. Moore, Phys. Rev. Lett. **90**, 127201 (2003)
32. J. Adler, Y. Meir, A. Aharony, A.B. Harris, Phys. Rev. B **41**, 9183 (1990)